COMMUNICATION

Supporting Information

Inkjet-printed co-continuous mesoporous oxides for high current power transistors

Nehru Devabharathi, Sandeep Kumar Mondal, Subho Dasgupta*

Department of Materials Engineering, Indian Institute of Science (IISc), C V Raman Avenue, Bangalore: 560012, Karnataka, India

*Email: dasgupta@iisc.ac.in

Contents

A. Atomic force micrographs of In_2O_3

Fine surface morphology of the single-layer printed In_2O_3 film has been studied using Bruker dimension icon atomic force microscope with silicon nitride tip having 15 nm tip radius. The sample preparation has been identical to the SEM samples. The obtained AFM image (Fig. S1 a) reveals that the oxide ligaments of the mesoporous structures are in fact polycrystalline in nature. The size of the particles appears a little bigger than that has been observed under HRTEM; however, this can be due to a smearing effect from the AFM tip used.

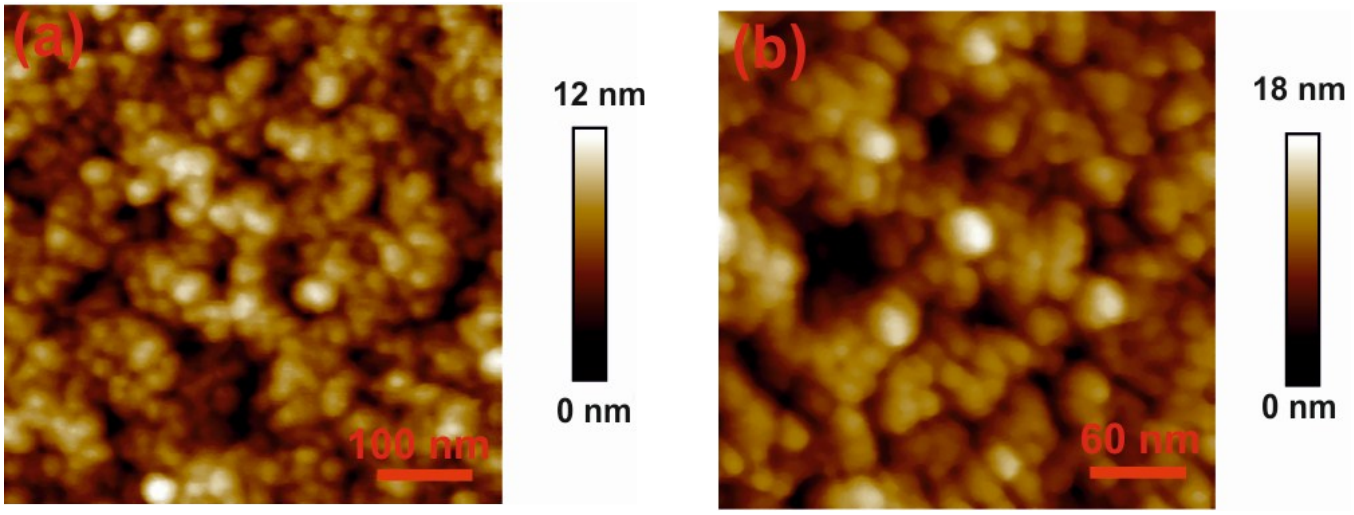

Fig. S1 (a-b) Atomic force micrographs of single layer printed In_2O_3 meso-structures. The scanned areas of the images are 500×500 nm^2 and 300×300 nm^2, respectively.

B. Cross-section SEM images of printed mesoporous In_2O_3 layers:

To estimate the thickness of the printed meso-structures, cross-section scanning electron microscopy has been carried out on single-pass and five-pass printed In_2O_3 films. The samples have been prepared by printing round of 250 µm size areas/ droplets and carefully sectioned to obtain a flat edge. The cross-section SEM images of 1 and 5 layers printed In_2O_3 films are shown in Fig. S2 (a-b). The thickness estimation from the cross-sectional SEM images stand at around 60 nm and 150 nm, for the 1 and 5 layer printed films, respectively.

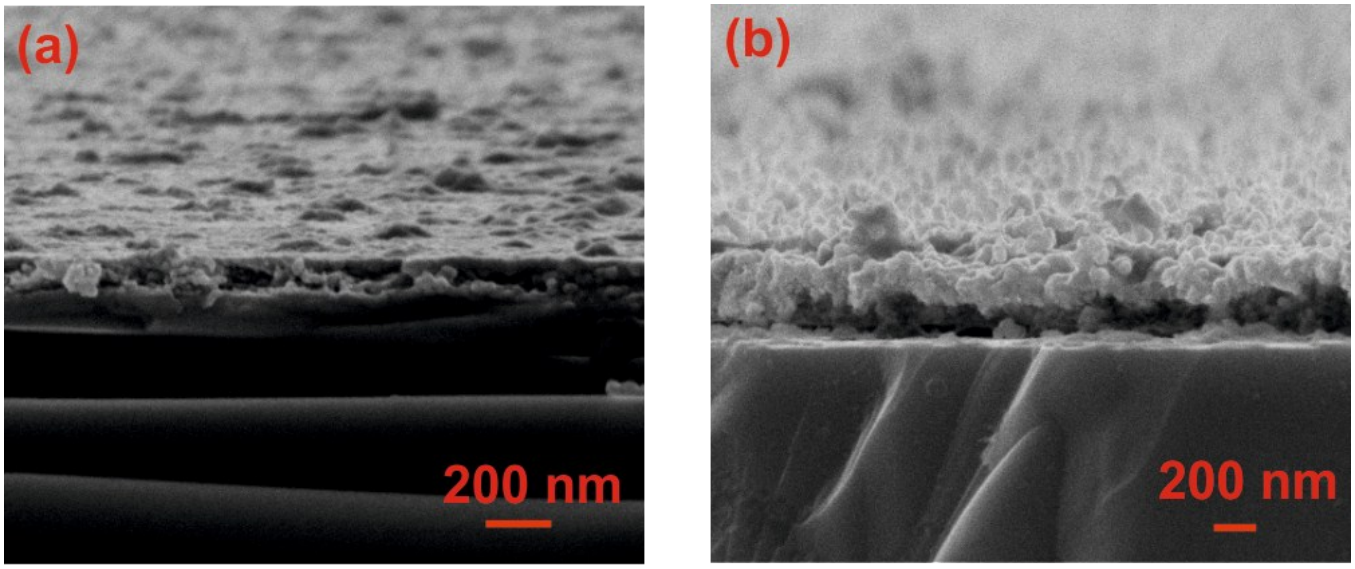

Fig. S2 (a-b) Cross-section scanning electron micrographs of single-pass and five-pass printed In_2O_3 layers, respectively.

C. Particle size histograms of SnO_2, In_2O_3 and ITO.

Estimation of accurate average particle size and size distribution has been carried out using the data extracted from the HRTEM images. Fig. S3 (a-c) shows the histogram of SnO_2, In_2O_3 and ITO with the average particle size of 4.5 nm, 10.2 nm and 10.6 nm respectively.

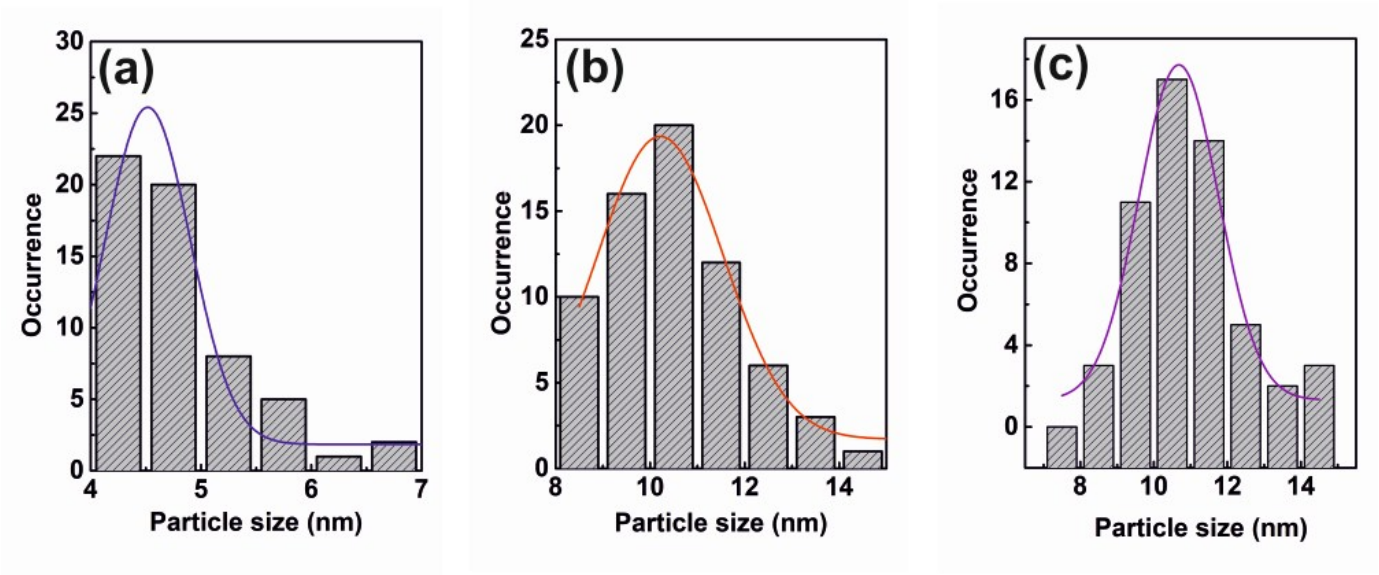

Fig. S3. (a-c) Particle size histograms of SnO_2, In_2O_3 and ITO with the average particle size of 4.5 nm, 10.2 nm and 10.6 nm, respectively.

D. STEM-mode EDX analysis of printed mesoporous oxide layers

The chemical analysis of the SnO_2 and ITO meso-structures has been carried out with EDX performed at STEM mode. In every case (Fig. S4 and S5), the first image shows a micrograph at STEM mode, while the second image is the micrograph with elemental mapping of the constituents and the remaining ones are only the elemental maps of the respective metals and oxygen.

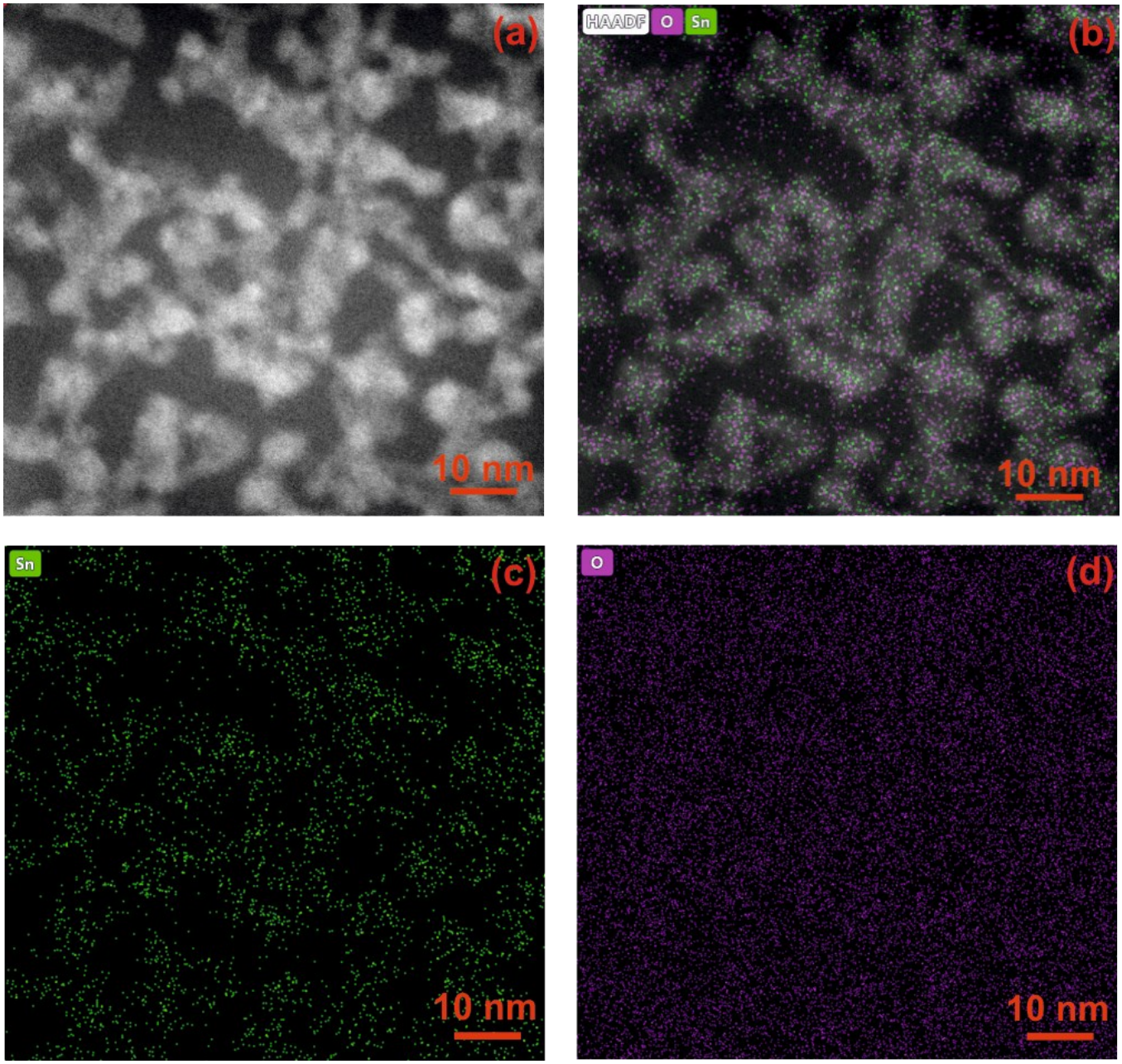

Fig. S4 (a) STEM image of the printed SnO_2 layer showing the ligament and pore distribution, (b) EDX elemental mapping (Sn, O) performed on the entire area, (c) elemental mapping of tin, (d) elemental mapping of oxygen.

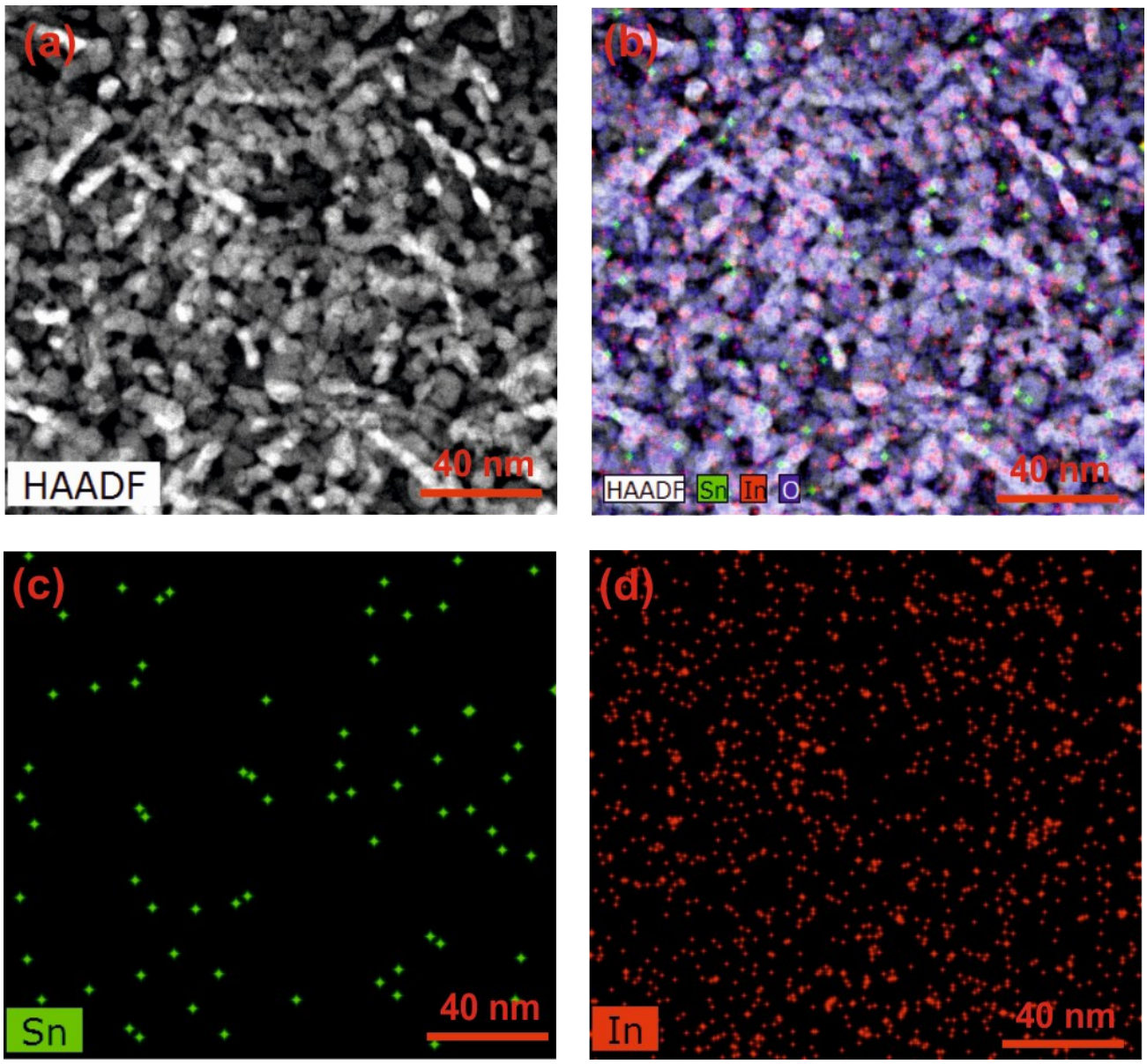

Fig. S5 (a) STEM image of the printed ITO layer showing the ligament and pore size distribution, (b) EDX elemental mapping (In, Sn, O) performed on the entire area, (c) elemental mapping of tin, (d) elemental mapping of indium.

E. Additional micrographs of mesoporous SnO_2 and In_2O_3 at lower magnification showing spatial homogeneity of the printed co-continuous porous layers

Fig. S6 shows additional microscopic (SEM and TEM) images of the single-layer printed SnO_2 (Fig. S6 a, c, d) and In_2O_3 (Fig. S6 b) mesostructure to reveal the co-continuous nature of the ligament and pore network at different length scales. In fact, all the different oxide mesostructures have been found to be highly homogeneous and isotropic even at the millimetre scale.

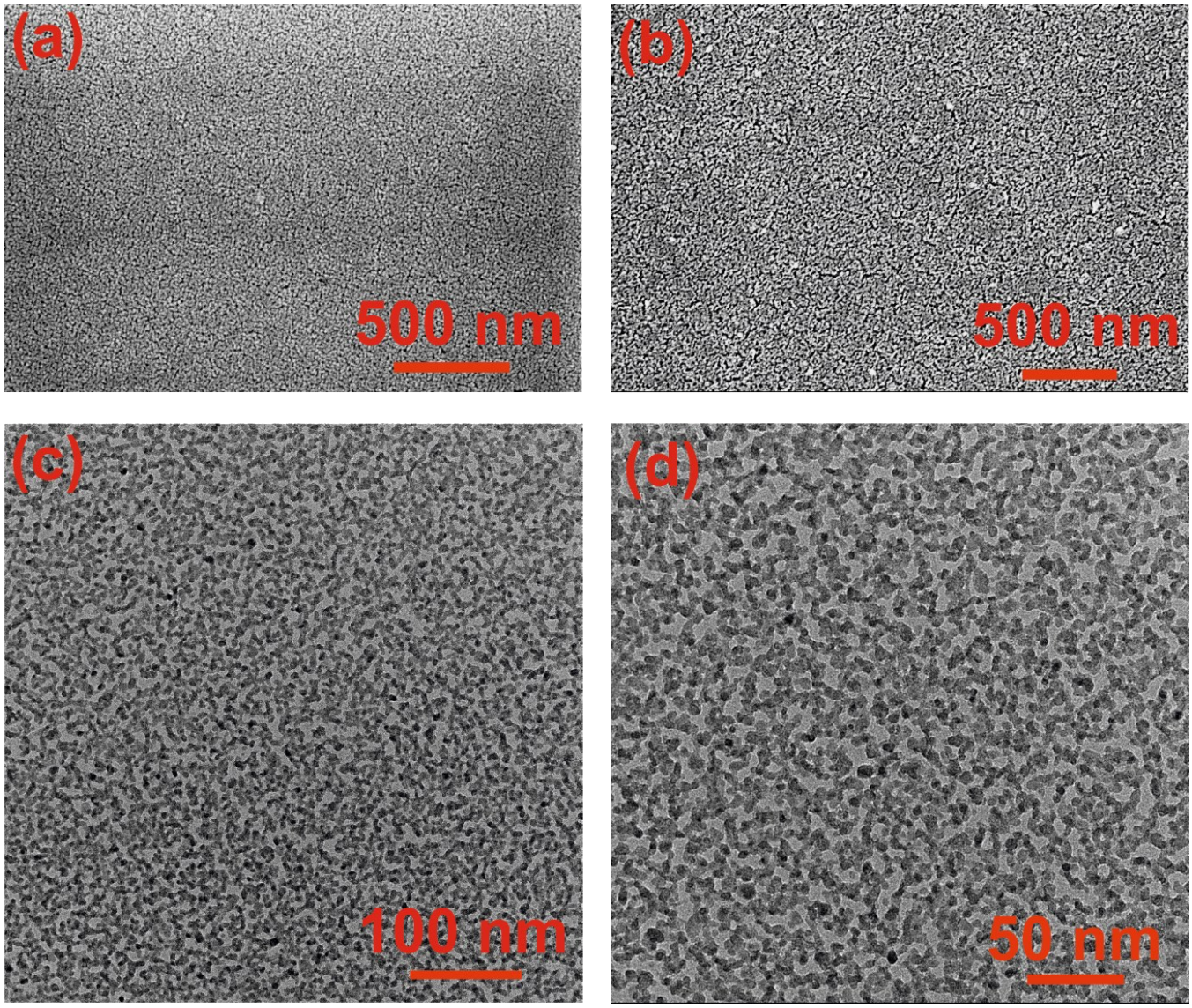

Fig S6 Scanning electron microscopy images of mesoporous (a) SnO_2 and (b) In_2O_3 at different magnification, showing co-continuous and isotropic nature of the mesoporous structure at a higher length scale; (c-d) additional TEM images of mesoporous SnO_2 at lower magnification.

F. Top-view of the FET geometry with printed silver to narrow down the channel dimensions

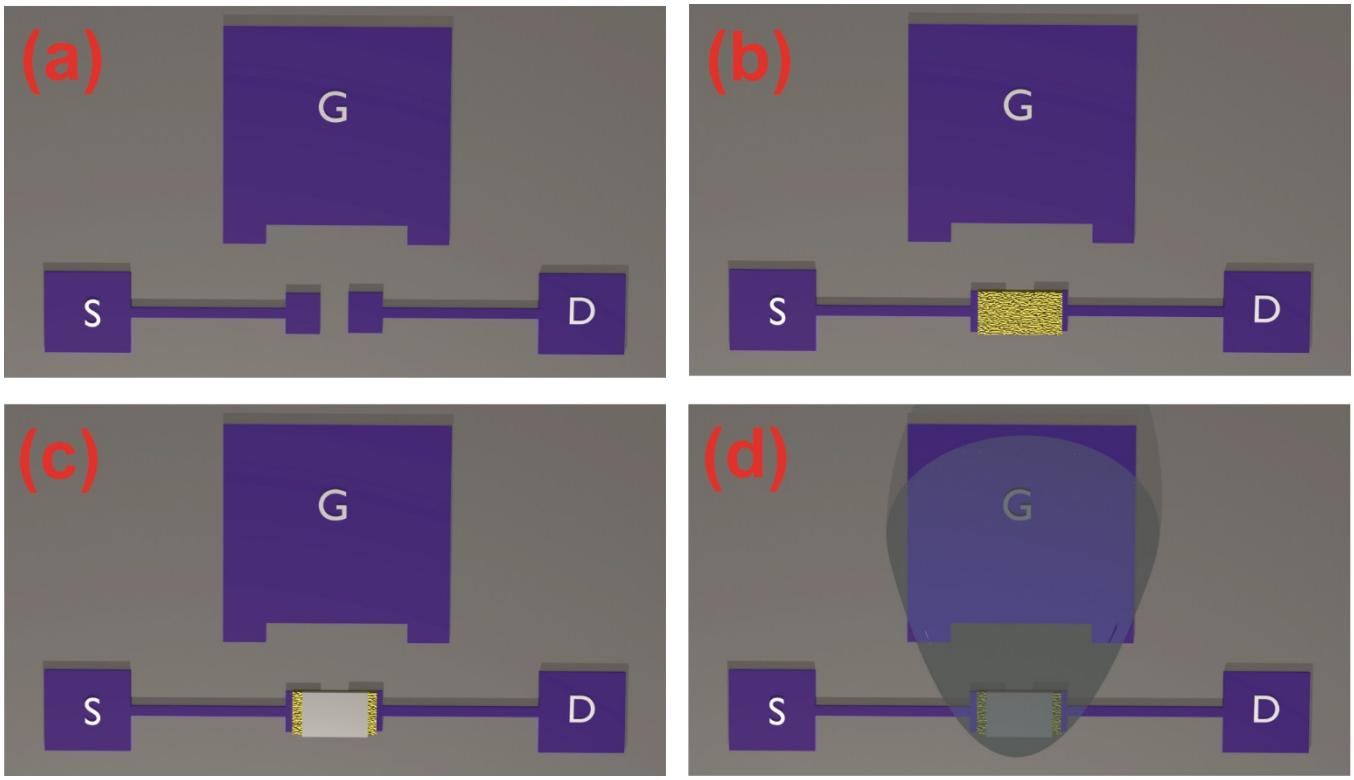

Fig S7 Top view of the in-plane/ displaced gate device geometry with printed silver layer on top of the mesoporous In_2O_3 channel: (a) ITO based, lithographically-defined passive electrodes, (b) Printed and annealed mesoporous indium oxide semiconductor to comprise the FET channel. (c) Printed additional silver layer on top of the FET channel layer. (d) The complete FET device with printed composite solid polymer electrolyte as the gate insulator.

G. Cross-section transmission electron microscopy image of the mesoporous In_2O_3 and electrolyte interface

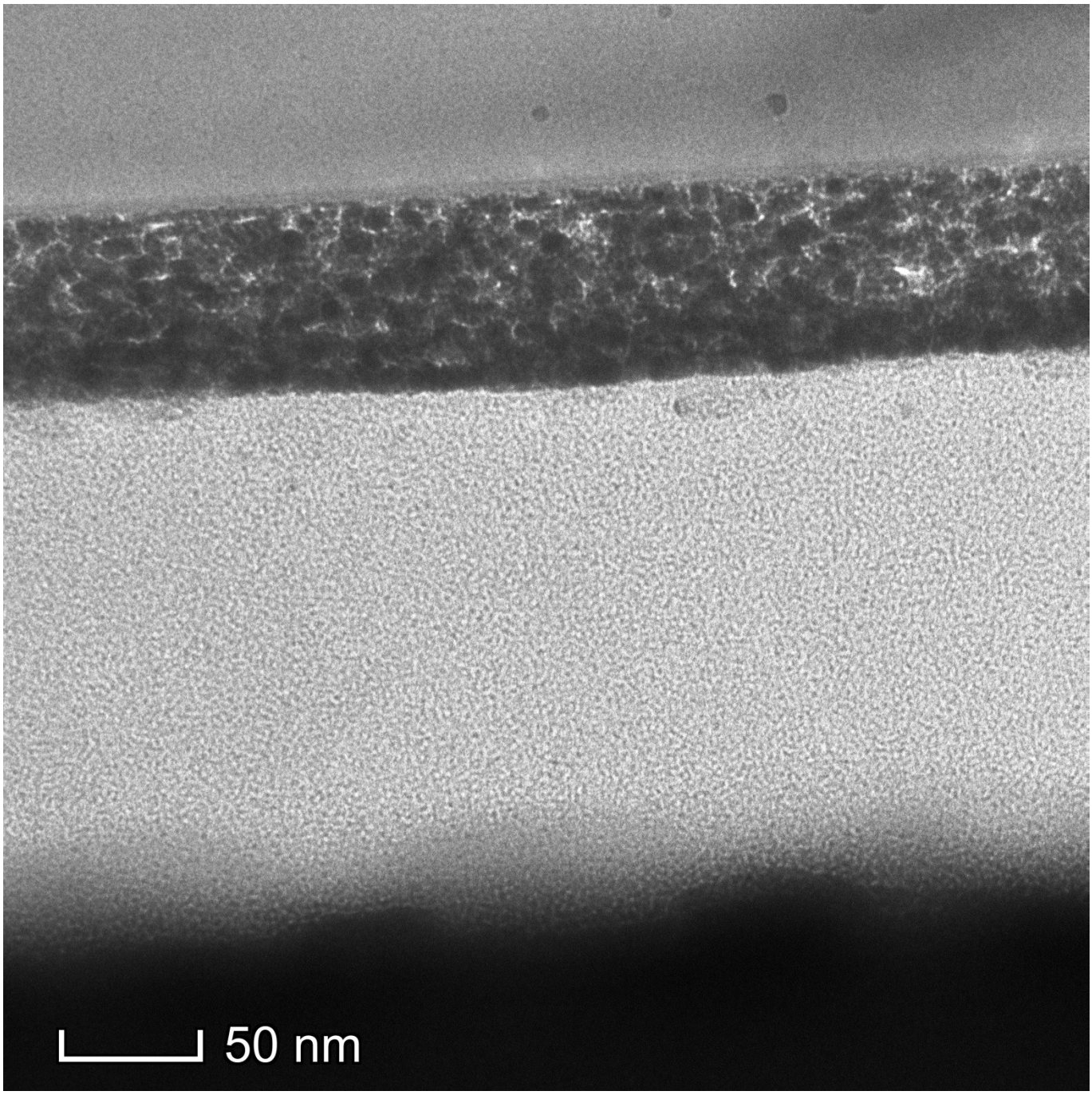

Fig. S8 CS-TEM image of the printed In_2O_3/ electrolyte interface; the bright amorphous region is the printed CSPE film, whereas the dark area at bottom is the deposited platinum layer.

H. Cross-section scanning tunnelling electron microscopy (STEM) image with energy dispersive X-ray spectroscopy (EDX) elemental mapping of the mesoporous In_2O_3 and electrolyte interface before the onset of the printed silver layer

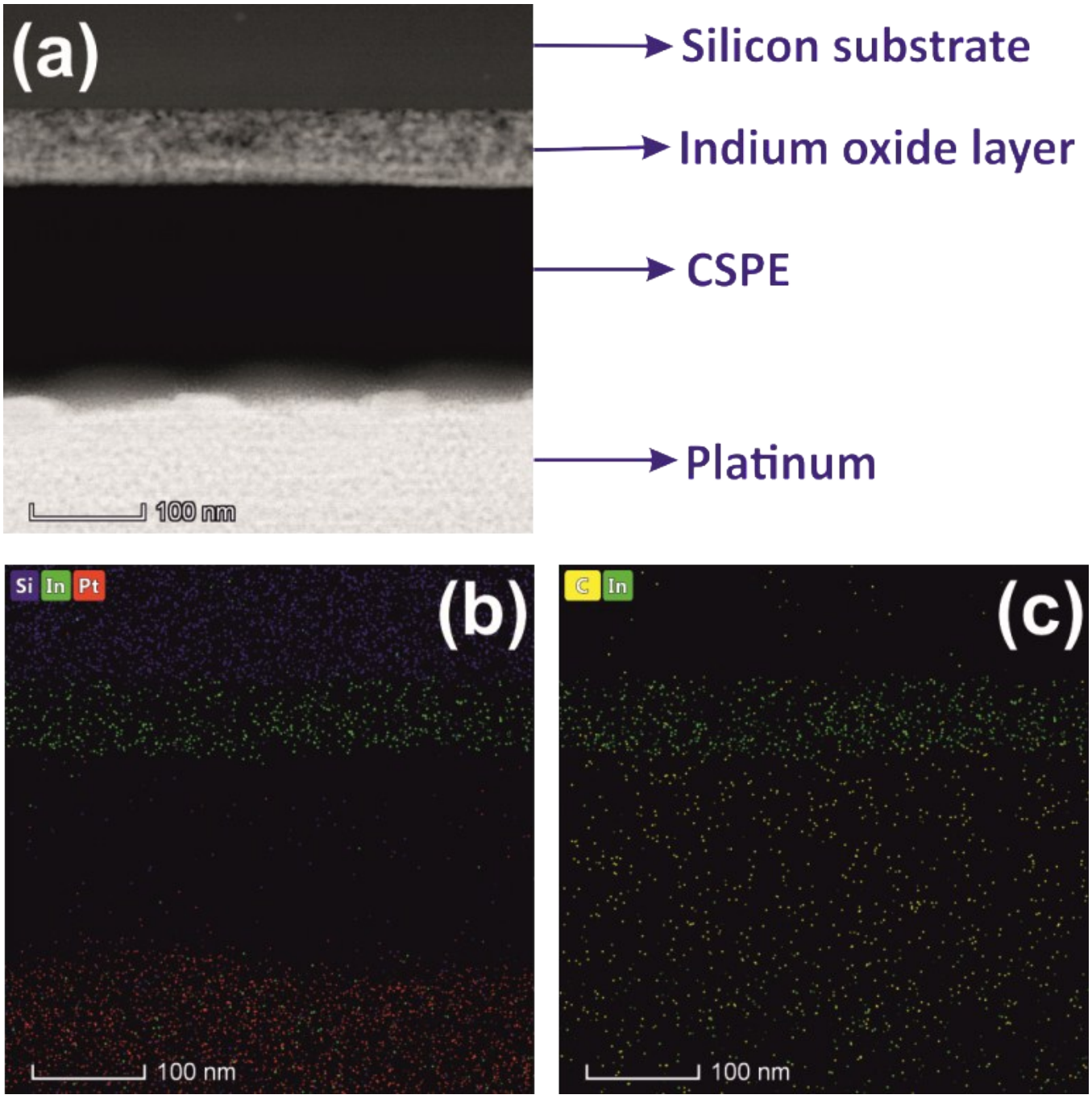

Fig. S9 (a) The high angle annular dark-field (HAADF) image of the In_2O_3/ electrolyte interface; (b) EDX elemental mapping showing the Si, In, Pt distribution; (c) EDX elemental mapping of In and C distribution.

The presence of significant carbon footprint within the mesoporous In_2O_3 layer ensures electrolyte penetration in the region.

I. Cross-section scanning tunnelling electron microscopy (STEM) image and energy dispersive X-ray spectroscopy (EDX) elemental mapping of the mesoporous In_2O_3 /silver/ electrolyte interface just after the onset of the printed silver layer

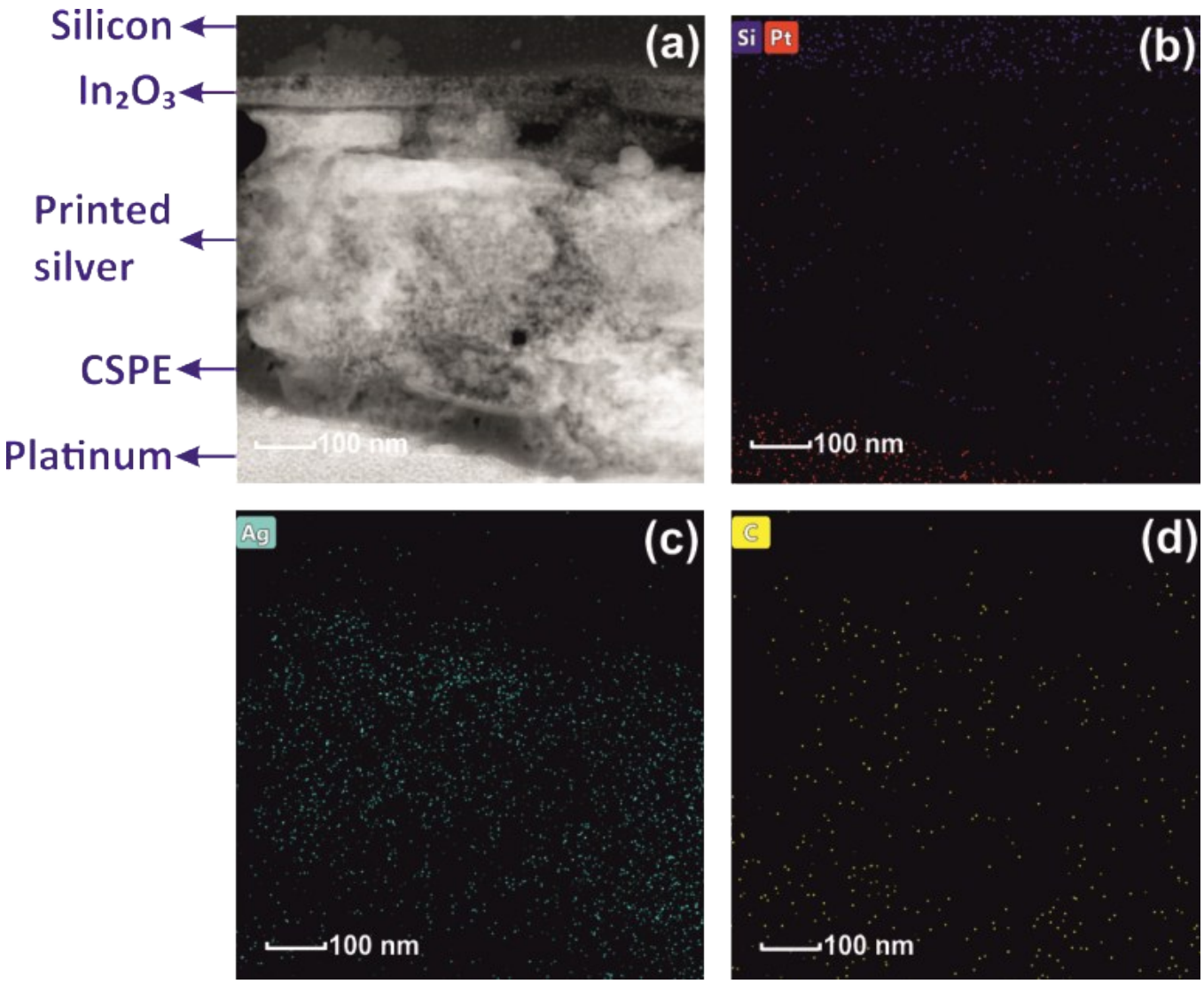

Fig. S10 (a) The high angle annular dark-field (HAADF) image of the In_2O_3/ silver/ electrolyte interface at the onset of the printed silver layer; (b) EDX elemental mapping showing the Si and Pt; (c) EDX elemental mapping showing Ag; (d) EDX elemental mapping showing C distribution.

The carbon footprint is fund to be weak in the mesoporous In_2O_3 layer underneath the printed Ag layer. The abundant carbon signal in the printed silver region is a result of the organic stabilizers and additives that have been used in the commercial nanoink.

J. Characteristic transconductance plot of the printed mesoporous In_2O_3/ silver- channel FETs and their average electrical performance parameters

The representative FET at the left panel shows On-state current density of 67 µA/µm and transconductance of 143 µS/µm, at a supply voltage of only V_{DS}= 0.5 V. The right panel summarizes the electrical performance parameters averaged on six FETs processed with identical printing and post-processing parameters.

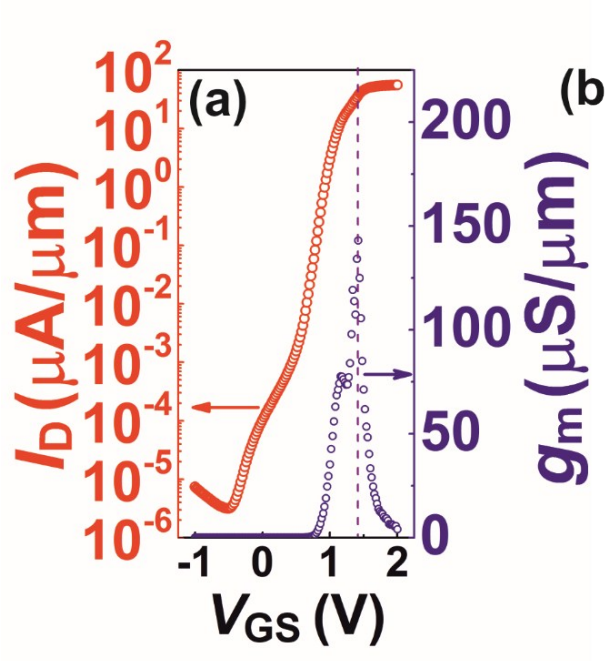

(b)

On/off ratio	$(1.4\pm0.27)\times10^7$
On current (µA/µm) at V_{DS} = 0.5 V	36.5±1.1
Off current (pA/µm)	2.5±0.33
Transconductance (µS/µm)	86.8±32.2

Fig. S11 (a) The transfer characteristics and transconductance of mesoporous In_2O_3/ silver channel FET, measured with applied drain voltage of V_D= 0.5 V; (b) the average electrical performance parameters are summarized.

K. Demonstration of lateral channel length independent drive currents of porous In_2O_3 channel FETs with the additional metal (silver) layer printed above the semiconductor channel

Here, two set of printed mesoporous In_2O_3/ silver channel devices have been fabricated and characterized within a single batch process. The chosen lithographically defined ITO channel lengths have been 10 and 40 μm, respectively, while the channel width has been kept constant. The observed drive currents at different drain voltages clearly indicate that the channel conductance is independent of the chosen lateral channel lengths of these transistors, as the transport through the semiconductor layer is effectively for a short vertical distance of the order of few tens of nanometers in each case. Moreover, this width normalized current density values compare favorably with any printed FETs reported till date.

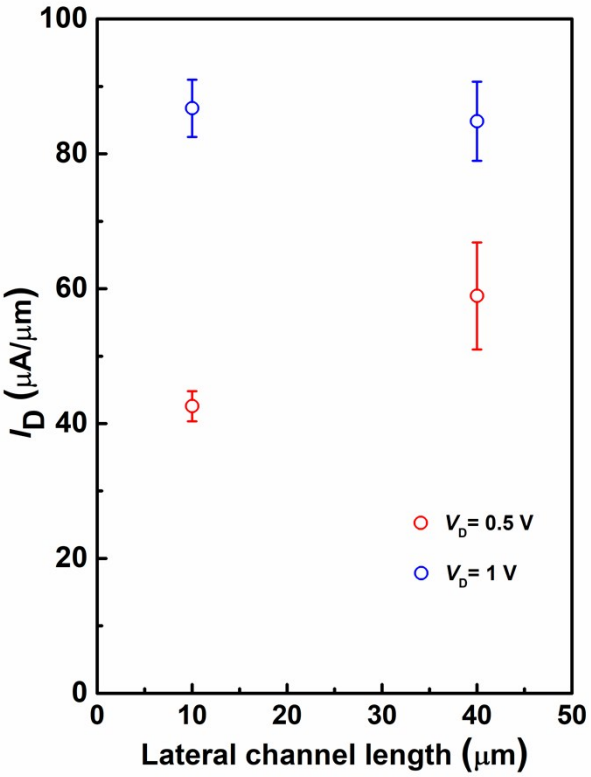

Fig. S12 The average On-currents with variability for a set of FETs fabricated with different lateral channel lengths than mentioned earlier in the manuscript (channel lengths defined by the ITO passives). The printed silver layer on top of the porous In_2O_3 channel makes the device current essentially independent of the lateral channel lengths.